COMMUNICATION

Coupling plasmonic catalysis and nanocrystals growth through cyclic regeneration of NADH

Received 00th January 20xx,
Accepted 00th January 20xx

DOI: 10.1039/x0xx00000x

Ana Sánchez-Iglesias,[a] Joscha Kruse,[b] Andrey Chuvilin[c,d] and Marek Grzelczak[b], *

In a typical colloidal synthesis, the molecules of the reducing agent are irreversibly oxidized during nanocrystal growth. Such scenario is of questionable sustainability when confronted with naturally occurring processes in which reducing agent molecules are cyclically regenerated. Here we show that cofactor molecules once consumed in the nucleation and growth of metallic nanocrystals can be photo-regenerated using metallic nanocrystals as photocatalyst and reused in the subsequent nucleation process. Cyclic regeneration of cofactor molecules opens up the possibilities for sustainable synthesis of inorganic nanoparticles.

In nature, biochemical cycles (*e.g.*, Krebs or futile cycles) are hidden driving force powering processes responsible for self-repair, growth or reproduction. In biocatalytic processes, cyclic reduction/oxidation of intermediate molecules (cofactors) is central in reaching high performance of technologically-relevant chemical transformations, either in batch[1] or in flow conditions.[2] Only recently has the concept of cycles attracted the attention of research community dealing with nanosystems. Thus, theoretical works have shown that periodic light energy delivery can accelerate the rate of templated self-replication of nanoparticles.[3,4] Experimental findings evidenced that cyclic assembly/disassembly of superlattices increases catalytic reaction rates under confinement.[5] Thus, switching from continuous to cyclic variant may favor the sustainability of existing (photo)chemical processes involving inorganic nanosystems by, for example, adapting to the diurnal cycle.

In a light-driven synthesis of plasmonic nanoparticles, the pre-formed nanoparticles act as both catalyst and seeds for the reduction of a metal precursor.[6–9] In such a process, photogenerated holes irreversibly oxidize the electron donor molecules (citrate[10] or alcohols[11]) while electrons reduce the metal precursor (gold, silver or palladium) exclusively on the nanocrystals surface.[9] As a result, the photocatalytic nanocrystals gain in size maintaining their total number, while the electron donor is irreversibly oxidized. We hypothesized that disentangling metal reduction and photocatalytic process by using recyclable reductor can leads to a scenario in which nanoparticles catalyze the formation of other nanoparticles of similar composition. Thus, the total number of nanoparticles can increase. Although light-induced growth of nanoparticles out of the surface of "mother" nanoparticles has been attained on solid substate[12,13] or in colloidal phase,[14] the processes described suffer from low efficiency because they were carried out with a continuous supply of light energy. Here we propose a cyclic variant of plasmonic catalysis, in which nanocrystals catalyze photoreduction of intermediate biomolecules that serve as reductor in the nucleation and growth of a new set of nanoparticles under dark conditions (**Figure 1**).

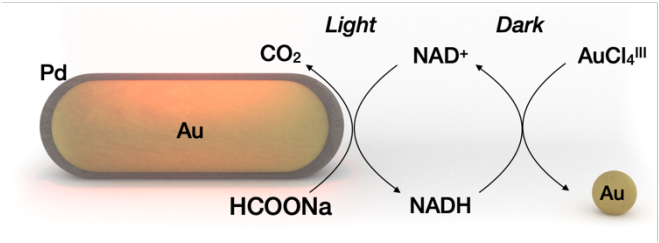

Figure 1. Cyclic photoregeneration of cofactor molecules allows plasmonic catalysis to be coupled to the nucleation and growth of metallic nanoparticles. In the light conditions, Au/Pd nanoparticles photocatalyst dehydrogenates sodium formate to NADH and CO_2 as a byproduct. In the dark conditions, NADH reduces metal precursor to gold nanoparticles. The light and dark processes can be performed cyclically.

The evaluation of our central hypothesis should take into account the following constrains: (i) Electron shuttle molecules are reversibly reduced by the metal photocatalyst and oxidized by the metal precursor. (ii) The reduced form of electron shuttle drives the nucleation of new nanoparticles in the dark, whereas other molecules in the medium (electron donor, stabilizer

[a] *Center for Cooperative Research in Biomaterials (CIC biomaGUNE), Basque Research and Technology Alliance (BRTA), 20014 Donostia – San Sebastián (Spain)*
[b] *Centro de Física de Materiales (CSIC-UPV/EHU) and Donostia International Physics Center, 20018 Donostia - San Sebastián (Spain), email: marek.g@csic.es*
[c] *CIC nanoGUNE BRTA, 20018 Donostia – San Sebastián (Spain)*
[d] *Ikerbasque Basque Foundation for Science, 48013 Bilbao (Spain)*
Electronic Supplementary Information (ESI) available: [details of any supplementary information available should be included here]. See DOI: 10.1039/x0xx00000x

molecules, byproducts) remain chemically inert. (iii) The molecules involved in dark reaction (*e.g.*, stabilizer) remain inert in the light reaction. (iv) Dark and light reactions require spatial separation to minimize back reactions (oxidation of the cofactor) and possible poisoning of the photocatalyst surface.

Nicotinamide adenine dinucleotide (NADH), which can be photoregenerated from NAD^+ on metallic nanocrystals, was chosen as an electron shuttle.[15–19] The standard redox potentials for the NAD^+/NADH and $AuCl_4^-/Au^0$ pairs are -0.32 V and 1.002 V, respectively, suggesting spontaneous gold reduction by NADH.[20,21] In addition, reduction/oxidation of NADH can be easily monitored optically, making it a suitable model electron shuttle. Sodium formate was chosen as an electron donor in the light process. Other groups have shown that sodium formate is a suitable electron donor for molecular hydrogen production on Pd-coated gold nanoparticles.[22,23] Our group has shown that dehydrogenation of sodium formate on Pd-coated gold nanoparticles can be coupled with regeneration of NADH.[18] On the other hand, metallic gold (here the product of dark reaction) is a poor catalyst for dehydrogenation of sodium formate,[24] ensuring dehydrogenation of sodium formate under light process only (requirement ii and iii). To physically separate the nanoparticle photocatalyst from the nanoparticle product, we chose to run the light reaction under flow conditions, while the dark reaction in batch.

The entire process is described as follows: Pd-coated gold nanorods catalyze photoregeneration of cofactor molecules (NAD^+ to NADH) using sodium formate as electron donor and producing CO_2 as a byproduct. In the subsequent dark reaction, NADH molecules promote the nucleation of metal precursor, forming gold nanocrystals. The oxidized redox mediator is recycled in the subsequent light process by physically separating the nanoparticles product from the mixture containing the oxidized cofactor (NAD^+). Throughout the process, light energy, formate ions and a metal precursor are the main ingredients for the synthesis of metallic nanoparticles using other metallic nanoparticles as a photocatalyst.

To demonstrate that the nucleation and growth of gold nanoparticles is driven by NADH (constrain ii), we performed time-resolved UV-vis-NIR measurements of the dark reaction by varying NADH:NAD^+ molar ratio ([NAD] = 1 mM, commercially available) in the presence of sodium formate (1M) at pH8. No metallic gold was observed at 100% of NAD^+, while at 100% of NADH the reduction was completed, forming nanocrystals of 2 nm diameter (**Figure 2 a,b,c**). Kinetic studies showed that the increase of localized surface plasmon resonance (LSPR) band at 510 nm is accompanied by the decrease of absorbance band at 340 nm, suggesting again that NADH is driving force in dark reaction (Figure S1). We found that NAD(H) interacts with the newly formed nanoparticles. The Z-potential of gold nanoparticles was -7 mV (Figure S2). The XPS analysis revealed the presence of N1s and P2p (Figure 2 d,e). These measurements suggest that NAD interacts with the gold surface through the nicotinamide moiety, corroborating previous results.[25] The NAD-Au interaction is further confirmed by photoluminescence of nanoparticles[26] through the emission band at 400 nm (Figure 2f). It should be noted that of NAD(H) retains chemical integrity during the dark reaction, as demonstrated by NMR analysis of the oxidized and reduced cofactor in the presence of metallic precursor (Figure S3).

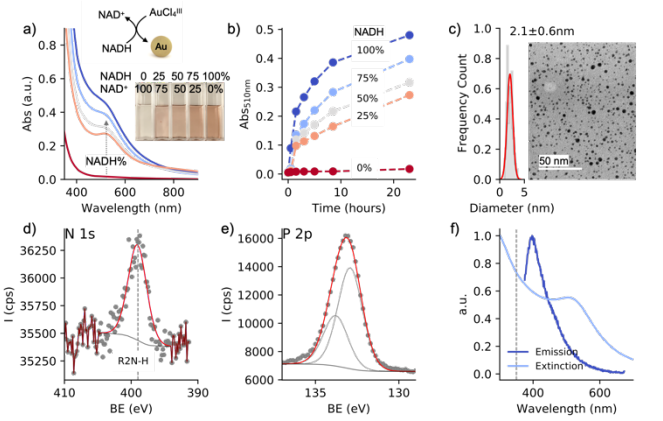

Figure 2. Dark reaction. a) effect of NADH : NAD^+ molar ratio on the nucleation of gold nanoparticles. Inset in a: digital images of nanoparticles solutions obtained at molar ratios ranging from 0 to 100 %. b) Time-dependent spectral change in solutions at different molar ratios. c) Size distribution and TEM image of nanoparticles obtained at 100 % NADH. d, e) XPS analysis showing the presence of nitrogen and phosphorous compounds in newly formed nanoparticles. f) Extinction and emission spectra of gold nanoparticles (excitation wavelength = 350 nm).

The use of conventional stabilizers - surfactant and polymer [27] – was ruled out because they interfered with light and dark reactions (*vide infra*). For example, cationic surfactant (*e.g.*, cetyltrimethylammonium bromide, CTAB) suppressed the photocatalytic activity of AuPd nanorods through their bromide content (Figure S4). In contrast, polyvinylpyrrolidone molecules induced non-selective nanoparticle nucleation even without NADH (Figure S5). In order to minimize the interaction of NAD with gold surface (and address constraint iii) we used sodium triphosphate (STTP), a chemically resistant compund (a food additive) that has been shown to have stabilizing properties on gold nanoparticles.[28]

We used palladium Pd-coated gold nanorods (length: 45.5±5.0 nm, width: 11.9±1.4 nm) as a plasmonic photocatalyst.[29–31] Upon Pd reduction on the surface of the gold nanorods, the maximum of LSPR redshifted from 735 to 763 nm (**Figure 3a**), indicating the formation of a metallic shell, which was confirmed by HRTEM analysis (Figure 3e and S6).

To gain processability of the photocatalyst without compromising optical properties, we immobilized AuPd nanorods on agarose beads (~100 µm).[32] The chemically rich agarose matrix interacts with the Au/Pd nanoparticles displacing the CTAB bilayer, without changing the optical properties of the nanoparticles even after thorough ethanol washing (Figure 3a). After immobilization, the LSPR shifted by ~25 nm due to an increase in the refractive index of the medium, as the refractive index of agarose is 1.34.[33] Thermogravimetric analysis showed that composite contains <1 wt% of photoactive metallic nanoparticles (Figure S7). Analysis of individual beads by darkfield microscopy revealed the presence of bright spots, the result of light scattering on the metallic element, which was not observed when using bare beads (Figure 3c and S8). The SEM analysis showed that AuPd

nanorods are randomly distributed on agarose beads (Figure 3d). The small interparticle distance, as observed on Figure 3d, is due to the shrinkage of highly porous agarose beads under vacuum. A combination of focused ion beam and SEM analysis allowed visualizing the distribution of AuPd nanoparticles in the beads. The nanoparticles were observed to distribute preferentially close to the surface of the agarose beads (Figure S9).

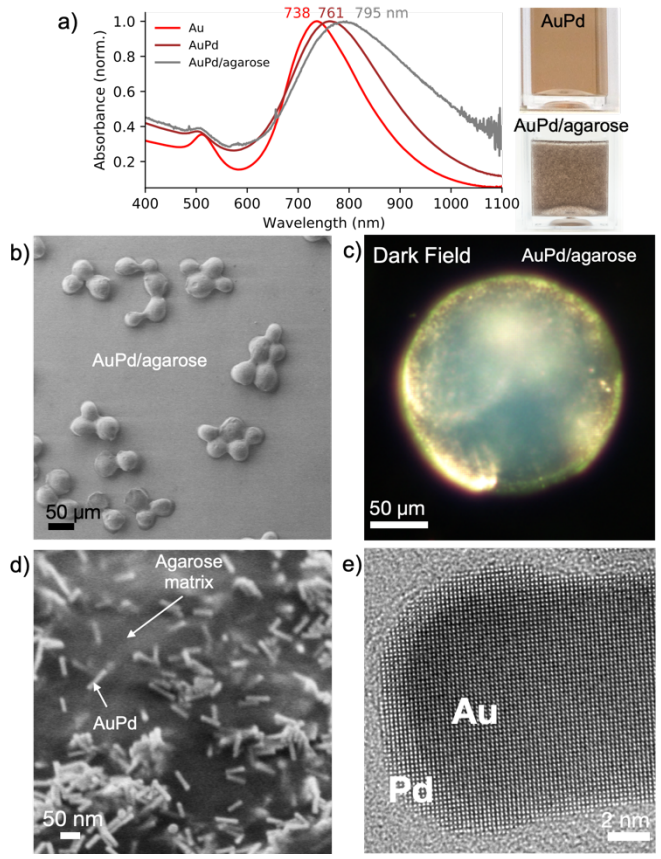

Figure 3. Plasmonic photocatalysts. a) UV-vis-NIR spectra of bare gold nanorods, Pd-coated and Pd-coated after immobilization in agarose beads. b) Low-resolution SEM image of AuPd/agarose. c) Dark Field image of individual beads (AuPd/agarose) with visible bright spots confirming the presence of plasmonic nanoparticles. d) SEM image of dried agarose bead showing randomly distributed AuPd nanorods. e) HRTEM image of AuPd nanorod with visible palladium shell.

To assess the simultaneous formation of NADH and CO_2 under light conditions, a photocatalyst placed at the bottom of the vial was irradiated for two hours (200 mW/cm^2, 400-1100 nm) (**Figure 4a inset**). The evolution of NADH was monitored in the liquid phase via UV-vis by measuring the absorbance at 340 nm. The formation of CO_2 was tracked in air phase through MS-GC chromatography (Figure 4a). These measurements confirmed the simultaneous regeneration of NADH and dehydrogenation of formic acid, confirming our previous results.[18] To further demonstrate the catalytic role of plasmonic nanoparticles we performed an action spectrum (7 wavelengths at 5 mW/cm^2 for 2h of irradiation) (Figure 4b), observing that NADH regeneration follows the AuPd/agarose spectral signature. Since dehydrogenation of formic acid is temperature dependent, we speculate that the plasmonic core favors a photothermal effect, which can be confirmed by the regeneration of NADH (2%) on bare gold nanorods (Figure S13).

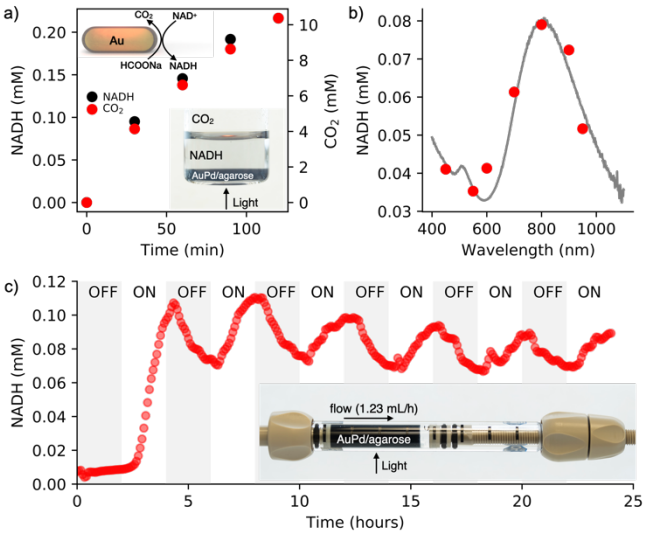

Figure 4. Light reaction. a) Time-dependent simultaneous evolution of NADH and CO_2 during light irradiation. Lower inset: digital image of batch photoreactor containing AuPd/agarose in the bottom. b) Wavelength-dependent regeneration of NADH. c) Photoregeneration of NADH in flow conditions, showing the change of NADH concentration at the outlet of the photoreactor upon ON-OFF light conditions. Inset: digital image of flow photoreactor during operation.

A facile processing the AuPd/agarose composite allows us to adapt batch photocatalysis to flow conditions. The flow photoreactor consisted of a column coupled at the outlet to an on-line UV-vis spectrophotometer to monitor the amount of regenerated NADH in real time (Scheme S1). Figure 4c shows the result of the light reaction run for 24 hours with alternating ON-OFF light states lasting 2 hours each. In the ON state, regeneration of NADH reached ~10%. The slight decrease in NADH concentration at longer times was presumably due to catalyst deactivation by evolved CO_2. The degradation of photoactive components (AuPd) inside the agarose matrix was excluded, which was confirmed by XPS analyses (Figure S10). Note that washing the beads out of the column once the reaction is completed allowed for recovery of the initial performance of the light process (Figure S11). Formic acid dehydrogenation and NADH reduction occur simultaneously on the photocatalyst surface. No NADH regeneration was observed when NAD^+ was supplied to the outlet of the photocatalyst column (Figure S12).

To evaluate our main hypothesis, we run three complete cycles of the light/dark reactions by supplying a mixture containing NAD^+ (0.001 M), sodium formate (1M), STTP (0.05 M) at pH8 the photoreactor (**Figure 5a**). To increase the efficiency of NADH regeneration, we doubled the light intensity (300 mW/cm^2), achieving ~55% of regenerated cofactor (Figure 5d). The collected mixture was combined with the gold salt and allowed to reduce the gold completely (Figure 5c).

Nanoparticles were separated from the mixture by centrifugal filtration and the collected permeate with the remaining NAD^+/NADH was delivered back to the flow photoreactor (Figure 5b). We observed a decrease in the amount of regenerated NADH with each subsequent light cycle, which is probably due to the interaction of the cofactor with the gold nanoparticles during the dark process or the interactions with agarose matrix (Figure 5f, red). We are also aware of $(NAD)_2$ formation,[34] as indicated by the remaining band at 340 nm after separation of nanoparticles from growth solution (Figure 5b). Consistently, the concentration of metallic gold also decreased with each cycle as the NADH:Au^{III} molar ratio of 4 was kept constant in each run. The diameter of the nanoparticles progressively decreased from 2.5 nm (firs cycle) to 1.8 nm (third cycle) (Figure 5e, S13). Since metal nanoparticles catalyze the formation of other metal nanoparticles by recycling the reducing agent, we estimated the turnover number as the ratio of the number of spherical nanoparticles product to the number of AuPd nanorods photocatalysts with each cycle. Given that photocatalytic bed contained $6x10^{12}$ nanorods and that after each cycle, the solution contained $6x10^{14}$, $8x10^{14}$, $7x10^{14}$ spherical gold nanoparticles, we estimated that one nanorod catalyzes the nucleation of 100, 133, and 117 spherical particles in each successive cycle (Figure 5f, black, Supporting Information – Section 12). These data show that cyclic recovery of cofactor allows plasmonic catalysis to be coupled to nucleation and nanoparticle growth, thus satisfying condition I.

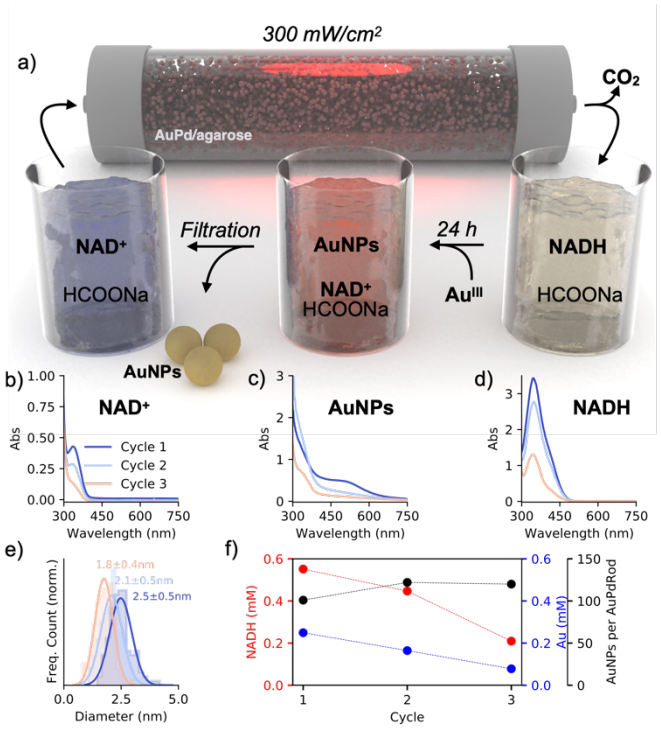

Figure 5. Coupling light and dark reactions through cyclic regeneration of cofactor molecules. a) Physical and temporal separation of light reaction in flow and dark reaction in batch. b-d) UV-vis spectra of (d) collected mixtures after light reaction, (c) mixture after dark reaction containing nanoparticles, (b) permeate solutions without nanoparticles before subsequent light reaction. e) Size distributions of nanoparticles after each dark process. f) Concentration of NADH (red), Au (blue) and ratio of new nanoparticles per AuPd nanorod (black) at each cycle. Despite the drop of NADH concentration, the number of new nanoparticles per one photocatalyst nanoparticles remains unchanged.

Conclusions

We provided a proof-of-concept experimental framework showing that cyclic photo-regeneration of cofactor molecules can link the process of plasmonic catalysis (light reaction) with the nucleation and growth of metallic nanocrystals (dark reaction). The prime difficulty of coupling the light and dark processes is to minimize the interference of a given component (stabilizer, electron donor) in the antagonistic reaction. Another difficulty is the creation of a positive feedback loop in which the dark reaction product would catalyze the subsequent light reaction, a property that is still missing in the present experimental framework. Note that the presence of Pd co-catalyst on gold nanorods was critical for the regeneration NAD^+ in the light reaction, making the new set of Au nanoparticles obtained in dark reaction unsuitable for photoregeneration of NADH. That is, metallic gold is unable to catalyze dehydrogenation of sodium formate. However, replacing palladium co-catalyst with (macro)molecular co-catalysts may overcome the issue related to the compositional similarity of mother and daughter nanocrystals and thus the conservation of photocatalytic activities over subsequent generations.

From a broader perspective, these results raise new promises on sustainable colloidal nanofabrication where nanoparticles by harvesting light energy catalyze the regeneration of their own reducing agent. Thus, future prospects envisage (i) the coupling the light and dark processes under batch conditions, (ii) the using of water as an electron donor to move closer to the creation of an artificial photosynthetic system.

Author Contributions

A.S.I and J.K – data curation, investigation, methodology, visualization, writing – review and editing; A.C – investigation, funding acquisition, resources, writing – review and editing; M.G. – conceptualization, funding acquisition, project administration, resources, methodology, validation, supervision, writing - original draft.

Conflicts of interest

There are no conflicts to declare.

Acknowledgements

This work was supported by the Spanish MINECO (PID2019-111772RB-I00) and BBVA Foundation -"Primera convocatoria de ayudas fundacion BBVA a investigadores, innovadores y creadores culturales." A.C. acknowledge support from Spanish MINECO under the Maria de Maeztu Units of Excellence Program (MDM-2016-0618). The authors thank Jordi LLop for the help with the measurements of CO_2 evolution, Daniel Padro

for help with the NMR analysis and Luis Yate for the assistance with XPS analysis.

References

1 S. Mordhorst and J. N. Andexer, *Nat. Prod. Rep.*, 2020, **37**, 1316–1333.
2 J. Britton, S. Majumdar and G. A. Weiss, *Chem. Soc. Rev.*, 2018, **47**, 5891–5918.
3 R. Zhang, D. A. Walker, B. A. Grzybowski and M. Olvera de la Cruz, *Angew. Chem. Int. Ed.*, 2014, **53**, 173–177.
4 F. Lugli and F. Zerbetto, *J Phys Chem C*, 2019, **123**, 825–835.
5 H. Zhao, S. Sen, T. Udayabhaskararao, M. Sawczyk, K. Kučanda, D. Manna, P. K. Kundu, J.-W. Lee, P. Král and R. Klajn, *Nat. Nanotechnol.*, 2016, **11**, 82–88.
6 A. Henglein and R. Tausch-Treml, *J. Colloid Interface Sci.*, 1981, **80**, 84–93.
7 R. Jin, Y. Cao, C. A. Mirkin, K. L. Kelly, G. C. Schatz and J. G. Zheng, *Science*, 2001, **294**, 1901–1903.
8 R. Jin, Y. Charles Cao, E. Hao, G. S. Metraux, G. C. Schatz and C. A. Mirkin, *Nature*, 2003, **425**, 487–490.
9 M. Grzelczak and L. M. Liz-Marzán, *Chem. Soc. Rev.*, 2014, **43**, 2089–2097.
10 X. Wu, E. S. Thrall, H. Liu, M. Steigerwald and L. Brus, *J. Phys. Chem. C*, 2010, **114**, 12896–12899.
11 Y. Zhai, J. S. DuChene, Y.-C. Wang, J. Qiu, A. C. Johnston-Peck, B. You, W. Guo, B. DiCiaccio, K. Qian, E. W. Zhao, F. Ooi, D. Hu, D. Su, E. A. Stach, Z. Zhu and W. D. Wei, *Nat. Mater.*, 2016, **15**, 889–895.
12 S. J. Lee, B. D. Piorek, C. D. Meinhart and M. Moskovits, *Nano Lett.*, 2010, **10**, 1329–1334.
13 E. Kazuma and T. Tatsuma, *J. Phys. Chem. C*, 2013, **117**, 2435–2441.
14 Y. Wei, S. Han, D. A. Walker, S. C. Warren and B. A. Grzybowski, *Chem. Sci.*, 2012, **3**, 1090–1094.
15 A. Sánchez-Iglesias, A. Chuvilin and M. Grzelczak, *Chem. Commun.*, 2015, **51**, 5330–5333.
16 A. Sánchez-Iglesias, J. Barroso, D. Martinez-Solis, J. M. Taboada, F. Obelleiro-Basteiro, V. Pavlov, A. Chuvilin and M. Grzelczak, *J. Mater. Chem. A*, 2016, **4**, 7045–7052.
17 K. Kinastowska, J. Liu, J. M. Tobin, Y. Rakovich, F. Vilela, Z. Xu, W. Bartkowiak and M. Grzelczak, *Appl. Catal. B Environ.*, 2019, **243**, 686–692.
18 N. Tarnowicz-Staniak, S. Vázquez-Díaz, V. Pavlov, K. Matczyszyn and M. Grzelczak, *ACS Appl. Mater. Interfaces*, 2020, **12**, 19377–19383.
19 S. Roy, V. Jain, R. K. Kashyap, A. Rao and P. P. Pillai, *ACS Catal.*, 2020, **10**, 5522–5528.
20 Y. Xiao, V. Pavlov, S. Levine, T. Niazov, G. Markovitch and I. Willner, *Angew. Chem. Int. Ed.*, 2004, **43**, 4519–4522.
21 L. Zhang, Y. Li, D.-W. Li, C. Jing, X. Chen, M. Lv, Q. Huang, Y.-T. Long and I. Willner, *Angew. Chem. Int. Ed.*, 2011, **50**, 6789–6792.
22 Z. Zheng, T. Tachikawa and T. Majima, *J. Am. Chem. Soc.*, 2014, **137**, 948–957.
23 B. Wu, J. Lee, S. Mubeen, Y.-S. Jun, G. D. Stucky and M. Moskovits, *Adv. Opt. Mater.*, 2016, **4**, 1041–1046.
24 X. Wang, Q. Meng, L. Gao, Z. Jin, J. Ge, C. Liu and W. Xing, *Int. J. Hydrog. Energy*, 2018, **43**, 7055–7071.
25 A. Damian and S. Omanovic, *Langmuir*, 2007, **23**, 3162–3171.
26 A. Bonanno, I. Pérez-Herráez, E. Zaballos-García and J. Pérez-Prieto, *Chem. Commun.*, 2020, **56**, 587–590.
27 Z. Zheng, T. Tachikawa and T. Majima, *J. Am. Chem. Soc.*, 2014, **136**, 6870–6873.
28 J. Xin, L. Miao, S. Chen and A. Wu, *Anal. Methods*, 2012, **4**, 1259–1264.
29 B. Nikoobakht and M. A. El-Sayed, *Chem. Mater.*, 2003, **15**, 1957–1962.
30 M. Liu and P. Guyot-Sionnest, *J. Phys. Chem. B*, 2005, **109**, 22192–22200.
31 M. Grzelczak, J. Pérez-Juste, B. Rodríguez-González and L. M. Liz-Marzán, *J. Mater. Chem.*, 2006, **16**, 3946–3951.
32 X. Ma, Y. Xia, L. Ni, L. Song and Z. Wang, *Spectrochim. Acta. A. Mol. Biomol. Spectrosc.*, 2014, **121**, 657–661.
33 E. Fujiwara, T. D. Cabral, M. Sato, H. Oku and C. M. B. Cordeiro, *Sci. Rep.*, 2020, **10**, 7035.
34 T. Saba, J. Li, J. W. H. Burnett, R. F. Howe, P. N. Kechagiopoulos and X. Wang, *ACS Catal.*, 2021, **11**, 283–289.